

Application of the efficient wave based prediction technique for the steady-state dynamic analysis of flat plates

B. van Hal, W. Desmet, D. Vandepitte and P. Sas

Department of Mechanical Engineering, division PMA, K.U.Leuven, Belgium
e-mail: bas.vanhal@mech.kuleuven.ac.be

Abstract

The use of the new wave based (*WB*) method, instead of the finite element (*FE*) method, for the steady-state dynamic response analysis of flat plates is considered. The mathematical background of the *WB* method is discussed in detail, where much attention is paid to the least-squares formulation. The comparison of both prediction techniques applied to an uncoupled plate problem illustrates the better convergence properties of the *WB* method with comparable computational costs. The introduction of a performance improvement further increases the computational efficiency of the *WB* method.

1. Introduction

The use of the finite element (*FE*) method ([1] and [2]) is generally accepted for dynamic response analyses. However, the *FE* method is practically limited to the low frequency range due to its computational costs, especially for coupled vibro-acoustic (*VA*) problems for which the system matrices are no longer symmetric. Recently, DESMET [3] has developed an alternative method for the dynamic analysis of *VA* systems, namely the wave based (*WB*) method, which exhibits better convergence properties than the *FE* method. VAN HAL *et al.* ([4] and [5]) show that, even for uncoupled plate problems, the *WB* method is a good alternative for the *FE* method.

In [4] and [5], the *WB* method is applied using a weighted residual formulation of the plate boundary conditions. This results in symmetric system matrices, but it requires the introduction of corner residual error functions. At the corner points of a plate, the normal and the tangential directions \vec{n} and \vec{s} are not uniquely defined (see figures 1 and 2). For corner points belonging to the clamped Γ_c or the simply supported boundary Γ_{ss} , the corner residual is the approximation error on the normal plate displacement at the corner point. In case of the free boundary Γ , the corner residual is the approximation error on the point force, associated with the discontinuity of the torsional moment T_s at the corner point. If coupled plate models are considered, it is difficult to determine the corner residual error functions. Therefore, the *WB* method, based on the least-squares formula-

tion, is preferred here, since this formulation does not require corner residual error functions. However, the system matrix, resulting from the least-squares formulation, is no longer symmetric, but hermitian. This paper illustrates that, also with the least-squares formulation, the *WB* can compete with the *FE* method.

Furthermore, this paper shows that some modification of the *WB* method improves its computational efficiency. This modification consists of the replacement of the numerical integration of the integrals in the system matrix by an exact integration, using analytical solutions.

The structure of this paper is as follows. First the mathematical background is discussed in section 2, followed by the comparison of the *WB* method and the *FE* method in section 3. Section 4 is concerned with the modification of the *WB* method. Finally, in section 5 the conclusions are summarized.

2. Mathematical background

2.1 Problem definition

The differential equation, describing the steady-state out-of-plane displacement response $w(\vec{r}) \cdot e^{j\omega t}$ of a flat plate subjected to a time-harmonic normal point force excitation $F \cdot e^{j\omega t}$ (see figure 1), is

$$(\Delta^2 - k_b^4) w(\vec{r}) = \frac{F}{D} \delta(\vec{r} - \vec{r}_F) \quad \text{in } \Omega \quad (1)$$

where $\Delta = \frac{\partial^2}{\partial x^2} + \frac{\partial^2}{\partial y^2}$ represents the Laplace operator, $k_b = \sqrt[4]{\frac{\rho t \omega^2}{D}}$ the plate bending wave number, $D = \frac{Et^3}{12(1-\nu^2)}$ the plate modulus, $\delta(\vec{r} - \vec{r}_F)$ the Dirac function, ρ the density, t the plate thickness, ω the circular frequency, E the Young's modulus and ν the Poisson constant. Three different types of boundary conditions (BC's) are considered, namely

1. clamped BC's at boundary Γ_c

$$w = 0, \quad L_\theta(w) = 0 \quad (2)$$

2. simply supported BC's at boundary Γ_{ss}

$$w = 0, \quad L_m(w) = 0 \quad (3)$$

3. free BC's at boundary Γ_f

$$L_m(w) = 0, \quad L_Q(w) = 0 \quad (4)$$

where L_* represent the linear operators defined as follows

$$L_\theta = -\frac{\partial}{\partial n} \quad (5)$$

$$L_m = -D \left(\frac{\partial^2}{\partial n^2} + \nu \frac{\partial^2}{\partial s^2} \right) \quad (6)$$

$$L_Q = -D \frac{\partial}{\partial n} \left(\frac{\partial^2}{\partial n^2} + (2 - \nu) \frac{\partial^2}{\partial s^2} \right) \quad (7)$$

with $\frac{\partial}{\partial n}$ and $\frac{\partial}{\partial s}$ the partial derivatives with respect to, respectively, the normal vector \vec{n} and the tangential vector \vec{s} at the boundary.

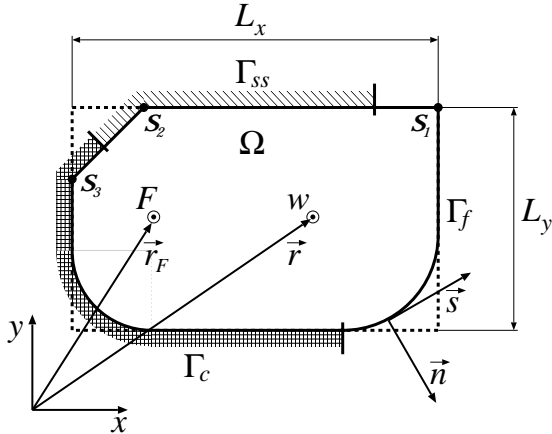


Figure 1: Flat convex plate subjected to harmonic excitation

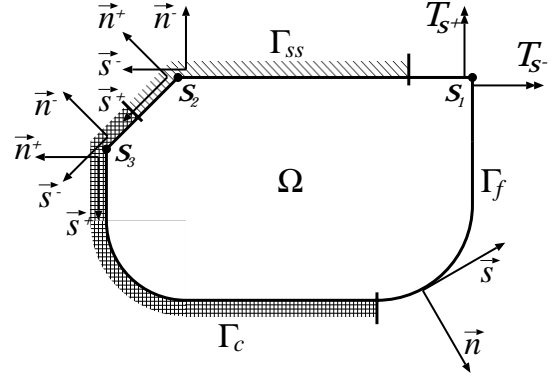


Figure 2: Corner point discontinuities

2.2 Response approximation

The deterministic *WB* technique, which is based on the indirect Trefftz approach [6], approximates $w(\vec{r})$ as a linear combination of wave functions $\Psi_a(\vec{r})$, extended by the particular solution $w_F(\vec{r} - \vec{r}_F)$

$$w(\vec{r}) \approx \hat{w}(\vec{r}) = \sum_{a=1}^{N_w} w_a \Psi_a(\vec{r}) + w_F(\vec{r} - \vec{r}_F) \quad (8)$$

$$\text{with } \Psi_a(\vec{r}) = \Psi_a(x, y) = e^{-j(k_{x,a}x + k_{y,a}y)} \quad (9)$$

$$\text{and } (k_{x,a}^2 + k_{y,a}^2)^2 = k_b^4 \quad (10)$$

where N_w represents the number of wave functions, w_a the wave contribution factor and $k_{x,a}$ and $k_{y,a}$ respectively the x - and y -component of the wave vector \vec{k}_a . The response of an infinite plate due to a normal point force excitation is selected as particular solution function

$$w_F(\vec{r} - \vec{r}_F) = -\frac{jF}{8k_b^2 D} \left(H_0^{(2)}(k_b \|\vec{r} - \vec{r}_F\|) + H_0^{(2)}(-jk_b \|\vec{r} - \vec{r}_F\|) \right) \quad (11)$$

where $H_0^{(2)}$ represents the zero-order Hankel function of the second kind.

2.3 Least-squares formulation

The approximation $\hat{w}(\vec{r})$ satisfies the differential equation (1) exactly, irrespective of the values of the unknown wave contribution factors w_a . Therefore only the BC's (2)–(4) determine the values of these factors. The violation of the BC's by the approximation function $\hat{w}(\vec{r})$ is minimized in an integral

sense. DESMET [3] considers two types of minimization schemes, namely the weighted residual formulation and the least-squares formulation. In [4] and [5], the weighted residual formulation is applied to the flat plate problem, but here the least-squares (LS) formulation is used.

The LS formulation requires the introduction of the following error functions R_*

$$R_w = \hat{w} \quad \text{on } \Gamma_c \cup \Gamma_{ss}, \quad (12)$$

$$R_\theta = L_\theta(\hat{w}) \quad \text{on } \Gamma_c, \quad (13)$$

$$R_m = L_m(\hat{w}) \quad \text{on } \Gamma_{ss} \cup \Gamma_f, \quad (14)$$

$$R_Q = L_Q(\hat{w}) \quad \text{on } \Gamma_f. \quad (15)$$

The functional \mathcal{F} , which is a measure for the total approximation error at the boundary Γ , is defined as

$$\begin{aligned} \mathcal{F} = & \alpha_w \int_{\Gamma_c \cup \Gamma_{ss}} \|R_w\|^2 d\Gamma + \dots \\ & + \alpha_\theta \int_{\Gamma_c} \|R_\theta\|^2 d\Gamma + \dots \\ & + \alpha_m \int_{\Gamma_{ss} \cup \Gamma_f} \|R_m\|^2 d\Gamma + \dots \\ & + \alpha_Q \int_{\Gamma_f} \|R_Q\|^2 d\Gamma \end{aligned} \quad (16)$$

in which the parameters α_* restore the homogeneity of the various parts of the functional \mathcal{F} . \mathcal{F} is minimized with respect to the unknown wave contribution factors w_a . This results in a set of N_w algebraic equations in the N_w unknown w_a 's represented by the wave model

$$\mathbf{A} \cdot \mathbf{w} = \mathbf{b} \quad (17)$$

where \mathbf{w} represents the column vector containing the unknown w_a 's. The wave model left hand side \mathbf{A} , which is hermitian, is given by

$$\begin{aligned} \mathbf{A}(a, b) = & \alpha_w \int_{\Gamma_c \cup \Gamma_{ss}} \Psi_a^c \Psi_b d\Gamma + \dots \\ & + \alpha_\theta \int_{\Gamma_c} L_\theta(\Psi_a^c) L_\theta(\Psi_b) d\Gamma + \dots \\ & + \alpha_m \int_{\Gamma_{ss} \cup \Gamma_f} L_m(\Psi_a^c) L_m(\Psi_b) d\Gamma + \dots \\ & + \alpha_Q \int_{\Gamma_f} L_Q(\Psi_a^c) L_Q(\Psi_b) d\Gamma \\ & \quad \forall a, b = 1, 2, \dots, N_w \end{aligned} \quad (18)$$

where Ψ_a^c represents the complex conjugate of Ψ_a .

The wave model right hand side \mathbf{b} is given by

$$\begin{aligned} \mathbf{b}(a) = & -\alpha_w \int_{\Gamma_c \cup \Gamma_{ss}} \Psi_a^c \hat{w}_F d\Gamma + \dots \\ & - \alpha_\theta \int_{\Gamma_c} L_\theta(\Psi_a^c) L_\theta(\hat{w}_F) d\Gamma + \dots \\ & - \alpha_m \int_{\Gamma_{ss} \cup \Gamma_f} L_m(\Psi_a^c) L_m(\hat{w}_F) d\Gamma + \dots \\ & - \alpha_Q \int_{\Gamma_f} L_Q(\Psi_a^c) L_Q(\hat{w}_F) d\Gamma \\ & \quad \forall a = 1, 2, \dots, N_w. \end{aligned} \quad (19)$$

2.4 WB model properties

The main advantages of the wave model (17) are

- the *small model size*, because the approximation \hat{w} satisfies a priori the plate equation (1), so only the boundary conditions (2)–(4) are violated and
- the *improved accuracy (with respect to the FE method) of the derived variables* (e.g. the stress), because the higher-order derivatives of $\Psi_a(\vec{r})$ (9) exhibit the same spatial variation as $\Psi_a(\vec{r})$ themselves.

The main disadvantages are

- the *fully populated system matrix \mathbf{A}* , because the wave functions $\Psi_a(\vec{r})$ are defined on the entire plate domain Ω (instead of an element domain for the *FE* method) and
- the fact that the *system matrix \mathbf{A} cannot be decomposed in frequency independent matrices* due to the implicit frequency dependence of the wave functions $\Psi_a(\vec{r})$.

2.5 Wave function selection

In order for the *WB* method to converge towards the exact solution, a complete set of wave functions is required. DESMET [3] proposes the following set of wave functions

$$\Psi_a(x, y) = \begin{cases} \cos(k_{x,p}x) \cdot e^{-j(k_{y,p}y)} \\ e^{-j(k_{x,q}x)} \cdot \cos(k_{y,q}y) \end{cases} \quad (20)$$

with their wave numbers according to

$$k_{x,p} = \pm \frac{p\pi}{L_x}, \quad k_{y,p} = \begin{cases} \pm \sqrt{k_b^2 - k_{x,p}^2} \\ \pm j \sqrt{k_b^2 + k_{x,p}^2} \end{cases}$$

$$k_{y,q} = \pm \frac{q\pi}{L_y}, \quad k_{x,q} = \begin{cases} \pm \sqrt{k_b^2 - k_{y,q}^2} \\ \pm j \sqrt{k_b^2 + k_{y,q}^2} \end{cases}$$

$$\forall p = 0, 1, \dots, n_p \quad \text{and} \quad \forall q = 0, 1, \dots, n_q \quad (21)$$

where L_x and L_y represent the dimensions of the (smallest) enclosing rectangle for the plate domain Ω (see figure 1).

DESMET [3] proves that a sufficient condition for the wave function selection (20) and (21) to converge is that Ω is convex. For non-convex domains a division in convex subdomains is required. For the practical implementation the complete set (21) is truncated for finite values of n_p and n_q . The following truncation rule is proposed (see [4])

$$n_p \geq \frac{k_b L_x}{\pi} \quad \text{and} \quad n_q \geq \frac{k_b L_y}{\pi} \quad (22)$$

which states that the plate bending wavelength $\lambda_b = 2\pi/k_b$ is not smaller than the smallest wavelength $\lambda = 2\pi/k$ of the truncated wave function set, with k the largest real value of the corresponding wave number set (21).

2.6 Numerical integration

To obtain the wave model (17), the complex integrals in (18) and (19) are numerically evaluated using the Gauss quadrature rule [7]. For large values of the wave vector components $k_{x,a}$ and $k_{y,a}$, the functions, which are integrated over the boundary Γ , show strongly oscillating spatial variations. This is illustrated by figure 3, which shows an example of the function $\Psi_a^c \Psi_b$ in equation (18). The wave vector components are implicitly dependent on the excitation frequency f through the frequency dependent plate bending wave number $k_b(f)$ in the wave function truncation rule (22). The $k_{x,a}$ and $k_{y,a}$ values increase for increasing frequency f . Therefore, the number of Gauss points n_{gp} is not constant during the numerical simulation, but it is made dependent on the largest absolute value of the wave vector components $k_{max} = \max(\|k_{x,a}\|, \|k_{y,a}\|)$. The following Gauss point selection rule is used

$$n_{gp} \geq 2k_{max}, \quad (23)$$

which states that at least 12 Gauss points are applied for the smallest wavelength of the truncated wave function set.

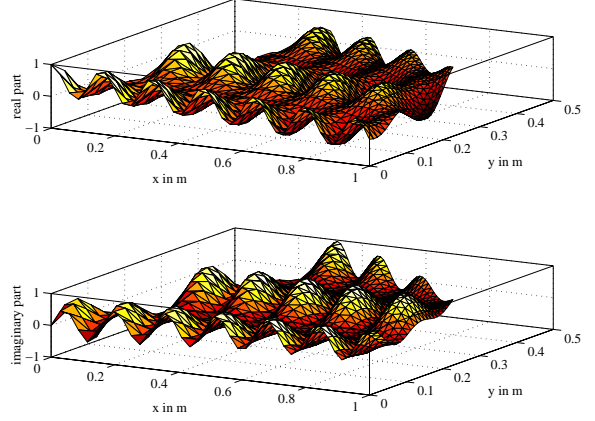


Figure 3: Function $\Psi_a^c \Psi_b$ to be integrated at 140 Hz:
 $\cos(6\pi x) \cos(4\pi y) e^{i(20.5779x + 15.0353y)}$

3. WB-FE comparison

3.1 Problem definition

A convex, clamped aluminum plate ($E = 70$ GPa, $\nu = 0.3$, $\rho = 2800$ kg/m³ and no damping) is considered with characteristic dimensions $L_x = 1.0$ m, $L_y = 0.5$ m and $t = 1$ mm (see figure 4). The objective is to predict the frequency response function (FRF) w/F between a point force excitation at $(\frac{1}{4}L_x, \frac{1}{4}L_y)$ and the displacement response at $(\frac{1}{2}L_x, \frac{1}{2}L_y)$. The frequency range of interest is $f \in [1, 200]$ Hz.

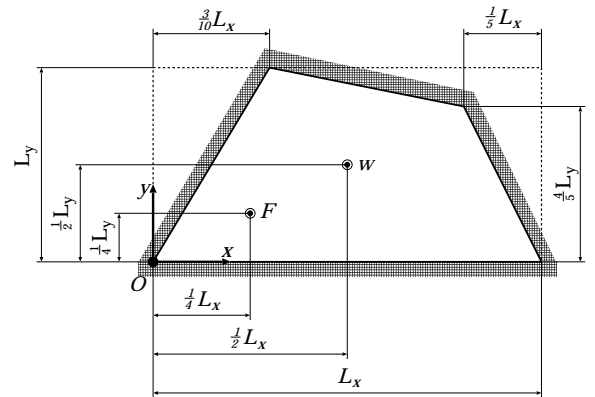


Figure 4: Convex, clamped aluminum plate

3.2 Model features

A wave model is built using truncation rule (22) and Gauss point selection rule (23). For $f \in [1, 200]$ Hz, the largest number of wave functions N_w is 124 and the largest number of Gauss points n_{gp} is 140. The parameters α_w and α_θ , which restore the homogeneity of the functional \mathcal{F} (see equation (16)), are given by

$$\alpha_w = \omega^2 \quad \text{and} \quad \alpha_\theta = \left(\frac{\omega}{k_b}\right)^2. \quad (24)$$

Three *FE* models are constructed with 8-noded quadratic plate bending elements [2]. The model *FE coarse* consists of 135 elements with 2270 degrees of freedom (dof's), the model *FE medium* consists of 240 elements with 3925 dof's and the model *FE fine* consists of 540 elements with 8585 dof's. Finally a *FE* model is generated with a very fine mesh, namely *FE reference* consisting of 1500 elements with 23305 dof's, for which the FRF prediction is assumed to be converged to the exact FRF within the frequency range of interest. The FRF prediction with this model is called the reference FRF.

3.3 Results

The computations are performed on a HP-UX 9000/780 machine. The *FE* predictions are obtained with MSC/NASTRAN, whereas the *WB* technique is implemented in the MATLAB environment. Figure 5 shows the results of both the *WB* FRF prediction and the *FE* FRF predictions. In the frequency range below 60 Hz, all FRF curves coincide. Above 60 Hz, the FRF prediction of the model *FE coarse* deviates from the reference FRF, whereas the FRF prediction with the models *FE medium*, *FE fine* and the *WB* model still are close to the reference FRF.

An indication of the accuracy of the *WB* method is obtained by inspection of the BC violation. One way to perform this inspection is by visualisation of the deformation pattern of the clamped plate as is for example shown in figure 6. At 140 Hz the BC's seem to be well satisfied based on this visual inspection.

Comparison of the relative errors of the displacement FRF's with respect to the reference FRF (see tables 1 and 2) shows, that the *WB* method possesses better convergence properties in terms of dof's than the *FE* method, as is already illustrated by DESMET [3]. However, comparison of the computational effort of both techniques shows, that the *FE* method is more efficient for the frequency range of interest. Note that

for the *FE* method only the CPU time for solving the dynamic matrix equation is taken into account, but not the CPU time to build the *FE* model, which is very short. The CPU time for the *WB* method includes the computational efforts of both building and solving the wave model. Figure 7 shows, that the computational costs for constructing the wave model is much higher than for solving the wave model. Furthermore, the CPU time for building the wave model increases for increasing frequency due to the higher number of both wave functions and Gauss points, which is required.

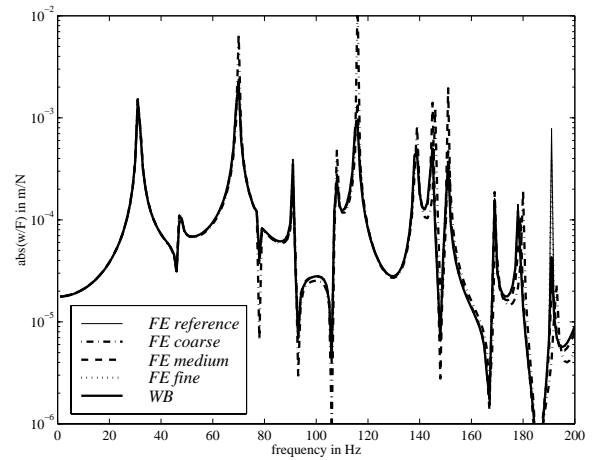


Figure 5: Comparison of *WB* and *FE* results

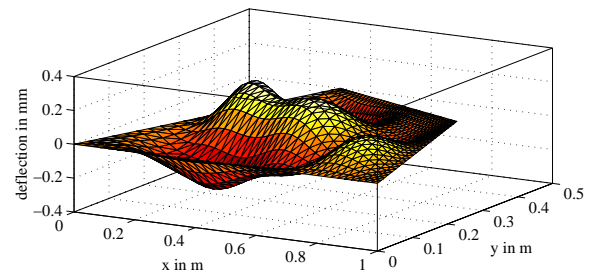


Figure 6: Deformation pattern at 140 Hz

model	no. of dof's	CPU time in s	relative error in %
<i>FE coarse</i>	2270	0.2	9.5
<i>FE medium</i>	3925	0.5	4.7
<i>FE fine</i>	8585	1.3	0.2
<i>WB</i>	124	3.3	0.6
<i>FE ref.</i>	23305	4.5	

Table 1: Properties of models at 140 Hz

model	no. of dof's	CPU time in s	relative error in %
<i>FE coarse</i>	2270	0.2	>25
<i>FE medium</i>	3925	0.5	12.3
<i>FE fine</i>	8585	1.3	1.1
<i>WB</i>	124	5.1	0.3
<i>FE ref.</i>	23305	4.5	

Table 2: Properties of models at 200 Hz

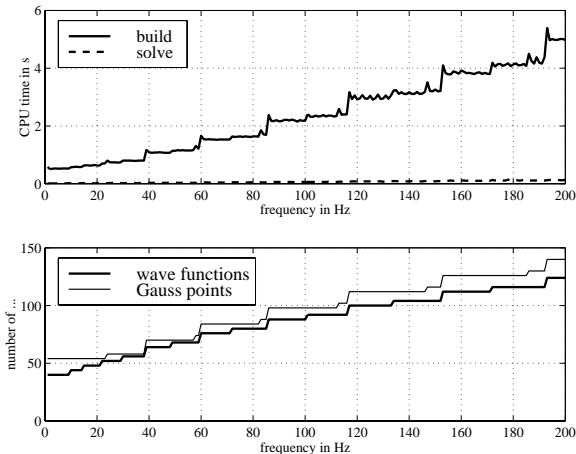


Figure 7: Properties of *WB* model

3.4 Conclusions

Although the *FE* method is more time efficient than the *WB*, its lack of accuracy for increasing frequency has to be compensated by the incorporation of a large number of dof's. This results in solution times comparable to those of the *WB* method, which has better convergence properties. Compare for example the CPU time of the *FE reference* model with the CPU time of the wave model (see table 2). If both the better convergence properties and the comparable computational efforts are taken into account, then the *WB* method forms a useful alternative for the *FE* method in steady-state dynamic analyses, certainly for increasing excitation frequency.

4. *WB* modification

4.1 Exact integration of \mathbf{A}

Figure 7 shows the increasing number of Gauss points required for higher frequencies f . This results in higher costs for the computation of each individual matrix entry of the wave model (17). Furthermore, the number of matrix entries increases, because more wave functions are taken into account (see figure 7).

In order to improve the computational efficiency of the *WB* method, analytical solutions for the complex integrals in the wave model matrix \mathbf{A} are implemented. The expressions for the analytical solutions are very extensive and are therefore omitted here, but in appendix A an example of such an expression is presented.

4.2 Accuracy check of numerical integration

The exact computation of the system matrix \mathbf{A} gives an indication of the accuracy of the numerical integration. If the FRF, obtained by computing \mathbf{A} exactly, is plotted in figure 5, then it coincides with the *WB* FRF. The relative errors between the predictions of both wave models at 140 Hz and 200 Hz are negligible ($\ll 1\%$). This proves, that application of the Gauss point selection rule (23) results in an accurate numerical integration.

4.3 Validation of *WB* modification

The implementation of the exact integration only affects the computational costs for building the wave model. Figure 8 summarizes these costs for both wave models. The comparison of the CPU times shows a decrease in efficiency. However, the number of floating-point operations (flops) with the exact integration is much smaller than the number of flops with the numerical integration. The implementation of the numerical integration is more straightforward than the implementation of the exact integration, which requires more conditional control statements (if-then-else). These conditional control statements have a bad influence on the efficiency within the MATLAB environment as is illustrated by the last plot in figure 8, showing the number of flops per CPU second. Other programming languages like FORTRAN and C do not exhibit this lack of efficiency due to conditional control statements. Thus the conclusion may be drawn, that the implementation of exact integration improves the computational efficiency of the *WB* method, although the CPU time increases within the MATLAB environment.

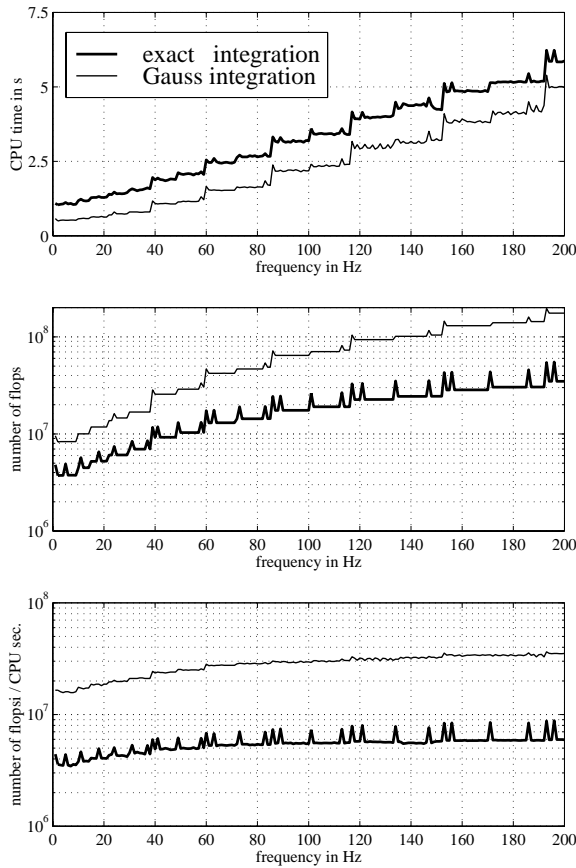


Figure 8: Validation of exact integration

5. Conclusions

In summary, there are two major conclusions:

1. The deterministic *WB* method can compete with the *FE* method for uncoupled steady-state dynamic analyses, also using the least-squares formulation instead of the weighted residual formulation. The *WB* method has better convergence properties with regard to the number of dof's, whereas the computational costs are comparable for increasing frequency.
2. The efficiency improves by the application of the exact integration for the wave model matrix **A**. The computational efficiency seems to suffer from the implementation of the exact integration, since the CPU time increases. However, the number of floating point operations (flops) decreases drastically. So the final conclusion is, that the application of the exact integration improves the computational efficiency of the *WB* method.

Acknowledgements

The research of B. van Hal is financed by a scholarship of the Institute for the Promotion of Innovation by Science and Technology in Flanders (IWT). W. Desmet is a Postdoctoral Fellow of the Fund for Scientific Research - Flanders (FWO).

References

- [1] O.C. Zienkiewicz. *The Finite Element Method - Vol. 1: Basic formulation and linear problems*. McGraw-Hill, London, 1977.
- [2] O.C. Zienkiewicz and R.L. Taylor. *The Finite Element Method - Vol. 2: Solid and Fluid Mechanics, Dynamics and Non-Linearity*. McGraw-Hill, London, 1991.
- [3] W. Desmet. *A wave based prediction technique for coupled vibro-acoustic analysis*. PhD thesis, KU Leuven, division PMA, 1998.
- [4] B. van Hal, P. Kobek, W. Desmet, and D. Vandepitte. Steady-state response analysis of a flat convex plate by the wave based prediction technique. In *Proceedings of the 5th National Congress on Theoretical and Applied Mechanics*, pages 87–90, Louvain-la-Neuve, 2000.
- [5] B. van Hal, W. Desmet, D. Vandepitte, and P. Sas. An efficient prediction technique for the steady-state dynamic analysis of flat plates. In *Proceedings of Inter-Noise 2000*, Nice, 2000.
- [6] E. Trefftz. Ein Gegenstück zum Ritzschen Verfahren. In *Proc. 2nd Int. Cong. Appl. Mech.*, pages 131–137, Zürich, 1926.
- [7] C.F. Gerald and P.O. Wheatley. *Applied Numerical Analysis*. Addison-Wesley Publishing Company, fourth edition, 1989.

A Exact integration

In section 4.1 it is already mentioned, that the expressions for the analytical solution of the entries in matrix **A** (see equation (18)) are extensive. Furthermore **A** is divided in four submatrices, because two different sets of wave functions are used (see equation (20)), namely

1. the p -set

$$\Psi_p(x, y) = \cos(k_{x,p}x) \cdot e^{-j(k_{y,p}y)} \quad (25)$$

2. and the q -set

$$\Psi_q(x, y) = e^{-j(k_{x,q}x)} \cdot \cos(k_{y,q}y). \quad (26)$$

The analytical solution for the first integral of submatrix \mathbf{A}_{pp} , where the boundary $\Gamma_c \cup \Gamma_{ss}$ is a straight curve with length L , is given by

$$\begin{aligned} \mathbf{A}_{pp}(a, b) &= \alpha_w \int_{\Gamma_c \cup \Gamma_{ss}} \Psi_a^c \Psi_b d\Gamma = \dots \\ &\frac{1}{2} \alpha_w (C_1(C_2 + C_3) + C_4(C_5 + C_6) + \dots \\ &\quad + D_1(D_2 + D_3) + D_4(D_5 + D_6)) \end{aligned} \quad (27)$$

with the constants C_* and D_* according to

$$\begin{aligned} C_0 &= C^2(k_{y,a}^c - k_{y,b})^2 - A^2(k_{x,a} + k_{x,b})^2 \\ C_1 &= -C_0^{-1} e^{j(k_{y,a}^c - k_{y,b})(CL+D)} \\ C_2 &= A(k_{x,a} + k_{x,b}) \sin((k_{x,a} + k_{x,b})(AL + B)) \\ C_3 &= jC(k_{y,a}^c - k_{y,b}) \cos((k_{x,a} + k_{x,b})(AL + B)) \\ C_4 &= C_0^{-1} e^{j(k_{y,a}^c - k_{y,b})D} \\ C_5 &= A(k_{x,a} + k_{x,b}) \sin((k_{x,a} + k_{x,b})B) \\ C_6 &= jC(k_{y,a}^c - k_{y,b}) \cos((k_{x,a} + k_{x,b})B) \\ D_0 &= C^2(k_{y,a}^c - k_{y,b})^2 - A^2(k_{x,a} - k_{x,b})^2 \\ D_1 &= -D_0^{-1} e^{j(k_{y,a}^c - k_{y,b})(CL+D)} \\ D_2 &= A(k_{x,a} - k_{x,b}) \sin((k_{x,a} - k_{x,b})(AL + B)) \\ D_3 &= jC(k_{y,a}^c - k_{y,b}) \cos((k_{x,a} - k_{x,b})(AL + B)) \\ D_4 &= D_0^{-1} e^{j(k_{y,a}^c - k_{y,b})D} \\ D_5 &= A(k_{x,a} - k_{x,b}) \sin((k_{x,a} - k_{x,b})B) \\ D_6 &= jC(k_{y,a}^c - k_{y,b}) \cos((k_{x,a} - k_{x,b})B) \end{aligned}$$

where the constants A , B , C and D are associated with the mapping of the line coordinate ξ along the boundary curve ($0 \leq \xi \leq L$) to the surface coordinates (x, y) , which is given by

$$\begin{aligned} x &= A\xi + B \\ y &= C\xi + D. \end{aligned} \quad (28)$$